REPORT ONR-CR212-249-2F

COMPUTATION OF THE TURBULENT MIXING IN CURVED EJECTORS

E. F. SCHUM
P. M. BEVILAQUA

Rockwell International
North American Aircraft Division
Columbus, Ohio 43216

S. V. PATANKAR

Department of Mechanical Engineering
University of Minnesota
Minneapolis, Minnesota 55455

CONTRACT N00014-78-C-0557
ONR TASK 212-249

30 APRIL 1980

INTERIM REPORT FOR PERIOD 1 SEPTEMBER 1978–31 AUGUST 1979

PREPARED FOR THE
OFFICE OF NAVAL RESEARCH • 800 N. QUINCY ST. • ARLINGTON, VA. 22217

Change of Address

Organizations receiving reports on the initial distribution list should confirm correct address. This list is located at the end of the report. Any change of address or distribution should be conveyed to the Office of Naval Research, Code 211, Arlington, VA 22217.

Disposition

When this report is no longer needed, it may be transmitted to other organizations. Do not return it to the originator or the monitoring office.

Disclaimer

The findings and conclusions contained in this report are not to be construed as an official Department of Defense or Military Department position unless so designated by other official documents.

Reproduction

Reproduction in whole or in part is permitted for any purpose of the United States Government.

UNCLASSIFIED

SECURITY CLASSIFICATION OF THIS PAGE (When Data Entered)

REPORT DOCUMENTATION PAGE

READ INSTRUCTIONS BEFORE COMPLETING FORM

1. REPORT NUMBER: ONR-CR212-249-2F	2. GOVT ACCESSION NO.: AD-A083905
3. RECIPIENT'S CATALOG NUMBER:	
4. TITLE (and Subtitle): COMPUTATION OF THE TURBULENT MIXING IN CURVED EJECTORS.	5. TYPE OF REPORT & PERIOD COVERED: Final Report. 1 Sept 78 - 31 Aug 79
	6. PERFORMING ORG. REPORT NUMBER: NR80H-11
7. AUTHOR(s): E. F. Schum, P. M. Bevilaqua, S. V. Patankar	8. CONTRACT OR GRANT NUMBER(s): N00014-78-C-0557
9. PERFORMING ORGANIZATION NAME AND ADDRESS: Rockwell International, ~~Corporation~~ North American Aircraft ~~Division~~ Columbus, Ohio 43216	10. PROGRAM ELEMENT, PROJECT, TASK AREA & WORK UNIT NUMBERS: 62241N; RF41-411-801; NR212-249
11. CONTROLLING OFFICE NAME AND ADDRESS: Office of Naval Research, Vehicle Technology Program (Code 211), Arlington, VA 22217	12. REPORT DATE: 30 April 1980
	13. NUMBER OF PAGES: 35
14. MONITORING AGENCY NAME & ADDRESS(if different from Controlling Office)	15. SECURITY CLASS. (of this report): Unclassified
	15a. DECLASSIFICATION/DOWNGRADING SCHEDULE

16. DISTRIBUTION STATEMENT (of this Report)

Approved for public release, distribution unlimited.

17. DISTRIBUTION STATEMENT (of the abstract entered in Block 20, if different from Report)

18. SUPPLEMENTARY NOTES

19. KEY WORDS (Continue on reverse side if necessary and identify by block number)

ejectors
V/STOL aerodynamics
turbulence
viscid/inviscid flow interactions
aircraft propulsion
thrust augmentation
jet flap diffuser

20. ABSTRACT (Continue on reverse side if necessary and identify by block number)

A numerical method has been developed to calculate the effects of curvature on the turbulent mixing within a thrust augmenting ejector. Curvature modification are included in both the kinetic energy and dissipation equations of the turbulence model. The elliptic effects of curvature on the mean flow are determined by combining an elliptic solution for the pressure field with a conventional marching solution for the velocity field. Predictions of the velocity profiles for jets and curved duct flows are compared with experimental data. Computation of the curvature effects are shown for an ejector

DD FORM 1 JAN 73 1473 EDITION OF 1 NOV 65 IS OBSOLETE

UNCLASSIFIED

SECURITY CLASSIFICATION OF THIS PAGE (When Data Entered)

401 390

having Coanda jets and one central jet.

TABLE OF CONTENTS

LIST OF FIGURES

LIST OF TABLES

NOMENCLATURE

a	convection and diffusion term defined by Equation (18)
A	convection and diffusion term defined by Equation (18)
Area	area used in the convection and/or diffusion flow
b	width of jet nozzle
BB	residual flow in the continuity equation, Equation (32)
C	convection rate, Equation (17)
c_1, c_2, c_μ	turbulence constants
d	diffusion rate defined by Equation (16)
D	diffusion or substantial derivative
E	nodal point E (Figure 3)
G	rate of generation of turbulent kinetic energy, Equation (9)
k	turbulent kinetic energy
ℓ	mixing length with curvature effects included
ℓ_o	mixing length in the absence of curvature effects
L	width of a channel
N	nodal point N (Figure 3)
P	pressure or nodal point, P (Figure 3)
r	distance in radial direction or radius
R_i, R_o	inner or outer radius
Re	Reynolds number
S	distance in the rθ direction or nodal point S (Figure 3)
$\overline{u'v'}$	Reynolds stress term
u'	turbulent fluctuation velocity in the U direction
U_{ℓ}	velocity in the S direction
"	velocity on centerline
$\hat{U}_P$, $\hat{U}_E$	terms used in the U momentum, Equations (24) and (25)
v'	turbulent fluctuating velocity in the V direction
v	velocity in the radial direction
$\hat{V}_N$ $\hat{V}_P$	terms used in the V momentum, Equations (27) and (28)
VOL	volume
w'	turbulent fluctuating velocity in a perpendicular direction from U and V
W	nodal point W (Figure 3)

x	distance from nozzle exit
y	distance measured from a wall (or centerline) in a channel (eg, Figure 6)
α	empirical constant used in Equation (2)
δ	distance used in diffusion equation, (Equation 16) or shear layer thickness (Equation 2)
ϵ	rate of dissipation of turbulent kinetic energy
θ	angle used in curvilinear coordinate system
μ	bulk viscosity
μ_t	turbulent viscosity
ρ	density
σ_k	Prandtl number for use in the turbulent kinetic energy equation (Equation 10)
σ_ϵ	Prandtl number for use in the turbulent dissipation equation (Equation 11)
Γ	symbolic notation used in Table I
ϕ	symbolic notation used in Table I
ω	angularity velocity

Subscripts

E	East
in	in.
jet	jet
max	maximum
N	North
out	out
P	at center
S	South
sec	secondary
W	West

Superscripts

u	for U momentum equation
v	for V momentum equation

INTRODUCTION

The U. S. Navy is considering several categories of V/STOL aircraft for use with smaller carriers, as a more economical means of maintaining sea control. One way of obtaining the additional thrust required by these aircraft is to divert the engine exhaust flow through a thrust augmenting ejector. Such an ejector is a kind of jet pump in which entrainment by the exhaust stream accelerates a larger mass of air drawn from the atmosphere. By Newton's law of action and reaction, the ejector experiences a force which is equal but opposite to the momentum change of the entrained air. A more complete description of this process has been given by Bevilaqua.[1]

Combining the ejector with the wing, as shown in Figure 1, produces an especially effective lift/propulsion system. A V/STOL aircraft having an

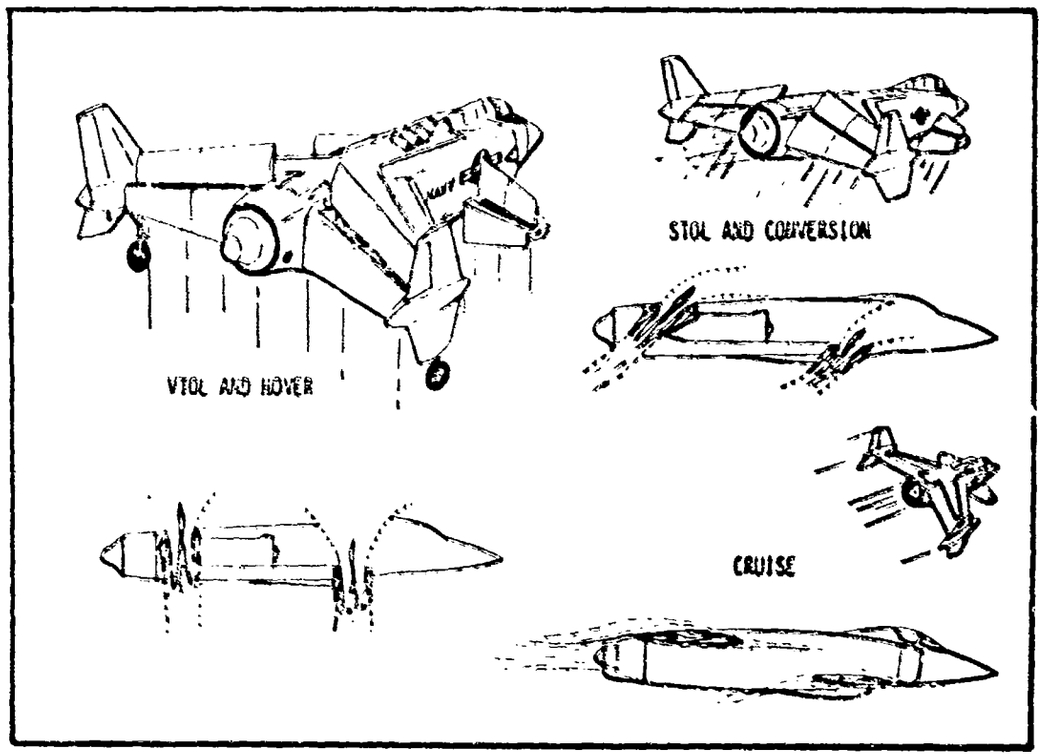

Figure 1. XFV-12A Integrated Lift/Propulsion System

ejector wing converts smoothly from jet-borne hover to wing-borne flight, because the wing lift is increased during conversion by the jet flap effect of the ejector exhaust stream. In addition, separate reaction jets are not required for control during hover; control forces may be generated by differential action of the ejectors. To demonstrate these advantages, the North American Aircraft Division of Rockwell International is developing the XFV-12A, a V/STOL aircraft which has ejectors in the wing and canard.

Although analytic methods for predicting ejector wing performance are necessary for conceptual design studies and to reduce test requirements, a theory for predicting both the lift and thrust of ejector wings has not been developed. There are methods for calculating the increments of aerodynamic lift and pitching moment induced by an ejector of given thrust. These are based on the now classical vortex sheet model of the pure jet flap devised by Spence.[2] Linearized, thin airfoil theories were developed for the ejector wing by Chan[3] and Woolard[4], who added a sink on the upper surface of a jet-flapped wing to represent entrainment by the ejector. Wilson[5] extended this approach by analyzing complete geometries, including thickness and camber as well as deflection of the jet wake. More recently, Mendenhall and McMillan[6] have begun investigation of three dimensional effects.

These methods have been useful in performing parametric analysis and for computing load distributions, such as surface pressures and hinge moments. However, neither the thrust augmentation ratio nor the initial thrust angle is predicted. In current practice, experimental data is used to specify the variation in these parameters during conversion from hover to conventional flight. Such an empirical approach is only useful for small variations from the original data base, so that there is no procedure for evaluating significant design changes or new configurations.

For static ejectors, Bevilaqua and DeJoode[7] developed a method of predicting the thrust augmentation by iterating between a viscous solution

for the turbulent mixing within the ejector and an inviscid solution for the flow outside the ejector. The purpose of this report is to describe a viscous solution developed for use in a similar analysis of the ejector wing. Calculating the turbulent mixing is more difficult in this case, because curvature effects become significant as the ejector is deflected aft. In the next section, the effect of curvature is discussed and the governing equations are presented. The numerical scheme devised to solve these equations is described in the following section. In the last section, the calculated results for some simple flow geometries are compared with available data, and a sample calculation for a typical ejector configuration is shown.

GOVERNING DIFFERENTIAL EQUATIONS

Mean Flow Equations

The performance of the ejector wing depends primarily on the thrust augmentation ratio and the thrust angle. However, computing these parameters is made difficult by the complexity of the ejector flow field. There are interacting regions of turbulent and irrotational flow, subject to lateral straining and streamwise curvature. The curvature produces strong lateral pressure gradients, which distort the inlet flow and deflect the thrust vector from the mean diffuser angle.

These elliptic effects due to curvature cannot be calculated with classical parabolic solution procedures,[7,8] in which upstream influences are neglected and the equations are solved by marching through the ejector in the streamwise direction. While a fully elliptic solution would include upstream influences, the requirements for increased computer storage and time make such an approach prohibitively expensive. Instead, we have adapted a method devised by Pratap and Spalding[9,10] for economically calculating upstream influences in duct flows. Since there is a primary direction of flow (through the duct) the elliptic effects are primarily due to transmission upstream by the pressure field. This type of flow falls between parabolic flows, in which there are no upstream influences, and elliptic flows, in which pressure, convection, and diffusion transmit influences in every direction. From a computational viewpoint, duct flows of this type may be classed as partly elliptic or partially parabolic.

The equations that govern the flow in the ejector are derived from Reynolds' equations for turbulent flows, by neglecting streamwise diffusion and upstream convection. Thus, the effect of a local disturbance is transmitted upstream by pressure only; downstream by pressure and convection; and across the flow by pressure, convection, and diffusion. In cylindrical coordinates

(r, θ) the governing equations take the form

Conservation of Mass

$$\frac{\partial U}{r\partial\theta} + \frac{\partial V}{\partial r} + \frac{V}{r} = 0$$

Streamwise Momentum

$$U \frac{\partial U}{r\partial\theta} + V \frac{\partial U}{\partial r} + \frac{UV}{r} = - \frac{1}{\rho} \frac{\partial P}{r d\theta} - \frac{\partial \overline{u'v'}}{\partial r} - \frac{2\overline{u'v'}}{r} \qquad (1)$$

Radial Momentum

$$U \frac{\partial V}{r d\theta} + V \frac{\partial V}{\partial r} - \frac{U^2}{r} = - \frac{1}{\rho} \frac{\partial P}{\partial r}$$

These equations do not describe the effect of curvature on the flow. The "extra" terms originate in the choice of coordinate system and do not imply any additional physical processes. The Coriolis acceleration, $UV/r = \omega V$ and the centrifugal acceleration $U^2/r = \omega U$, arise from rotation of the velocity vector with respect to the coordinate system. Similarly, the extra stress term is a consequence of having chosen a cylindrical volume element; that is, since the sides of the element are not parallel, the shear stress has a component, $\overline{u'v'}/r$, in the streamwise direction. Thus, the use of cylindrical coordinates is a convenience in this case, and the additional terms merely account for the difference between the actual accelerations of the fluid and those which appear to take place in the curvilinear coordinate system.

Turbulence Model

The effect of curvature is to increase the turbulent mixing rate. The first attempts to model this effect were straightforward extensions of mixing length theory. Prandtl[11] and Townsend[12] developed relations to increase the mixing length as the radius of curvature decreased. These had the general form

$$\ell = \ell_0 \left(1 + \alpha \frac{\delta}{r}\right) \qquad (2)$$

in which ℓ is the mixing length, δ is the shear layer thickness, and α is an empirical constant. This approach significantly underpredicts the change in the mixing rate. Bradshaw[13] improved this model by making the mixing length increase in proportion to the strain rate due to curvature,

$$\ell = \ell_o \left(1 + \alpha \frac{U/r}{\partial U/\partial r}\right) . \tag{3}$$

More recent proposals have been based on the turbulence kinetic energy equations. According to the usual eddy viscosity assumption, the turbulent stress is first expressed in terms of a turbulent viscosity, μ_t, and the mean strain rates

$$\overline{u'v'} = \mu_t \left(\frac{\partial U}{\partial r} - \frac{U}{r}\right) . \tag{4}$$

Again, no new physical process is implied by the extra strain rate, U/r. Following Launder and Spalding[14] the turbulent viscosity is assumed to depend on two parameters: the turbulence kinetic energy, k, and its rate of dissipation, ϵ. From dimensional arguments, the expression for the turbulent viscosity is

$$\mu_t = \frac{c_\mu \rho k^2}{\epsilon} \tag{5}$$

in which c_μ is an empirical constant.

Under the partially parabolic flow assumptions, the curvature equations for the three components of the turbulence kinetic energy take the following forms:

Change = Production - Dissipation + Diffusion + Rotation

$$\rho \frac{Du'^2}{Dt} = C - \frac{1}{3}\rho\epsilon + \frac{1}{3}D - \overline{u'v'}\frac{2U}{r}$$

$$\rho \frac{Dv'^2}{Dt} = - \frac{1}{3}\rho\epsilon + \frac{1}{3}D + \overline{u'v'}\frac{2U}{r} \tag{6}$$

$$\rho \frac{Dw'^2}{Dt} = - \frac{1}{3}\rho\epsilon + \frac{1}{3}D$$

In contrast to the mean flow equations, these turbulence equations contain additional terms which do represent a physical process caused by the curvature. Since the extra terms have opposite signs in the equations for u' and v', the effect of curvature may be interpreted as an eddy rotation which transfers energy from the streamwise component of the turbulence to the transverse component. This interpretation of the curvature terms was suggested by Hunt and Joubert.[15]

Summation of these three equations gives the equation for the turbulence kinetic energy, $k = \frac{1}{2}(u'^2 + v'^2 + w'^2)$ used by Launder and Spalding:[14]

$$\rho U \frac{\partial k}{r\partial\theta} + \rho V \frac{\partial k}{\partial r} = D + G - \rho\epsilon \tag{7}$$

Because the rotation simply transfers energy without loss between the turbulence components, curvature is seen to have no effect on the total turbulence energy. Thus, the classical turbulence energy equation cannot be used to determine curvature effects.

Instead, we have used a hybrid equation, which simulates the actual physical mechanism. The turbulence kinetic energy is used to provide an estimate of the average intensity of the velocity fluctuations which cause the turbulent mixing. However, in thin shear layers it is the v' component of the turbulence which produces most of the mixing. Therefore, an additional production term was added to the turbulence energy equation to represent the increase of v' due to curvature. The equation for the turbulence kinetic energy therefore becomes

$$\rho U \frac{\partial k}{r\partial\theta} + \rho V \frac{\partial k}{\partial r} = D + G - \rho\epsilon + \overline{u'v'}\frac{2U}{r} \tag{8}$$

in which G is the production of turbulence kinetic energy which occurs in the streamwise component. It has the form

$$G = \overline{u'v'}\left(\frac{\partial U}{\partial r} - \frac{U}{r}\right) \tag{9}$$

The expression for the diffusion of energy by the turbulent fluctuations is

$$D = \frac{\partial}{\partial r}\left(\frac{\mu_t}{\sigma_k}\frac{\partial k}{\partial r}\right) \tag{10}$$

An equation derived by Chambers and Wilcox[27] was used to compute ϵ, the dissipation of the turbulence energy. It contains the same curvature convection as the turbulence energy equation:

$$\rho U \frac{\partial \epsilon}{r d\theta} + \rho v \frac{\partial \epsilon}{\partial r} = (c_1 G - c_2 \rho \epsilon)\frac{\epsilon}{k} + \frac{\partial}{\partial r}\left(\frac{\mu_t}{\sigma_\epsilon}\frac{\partial \epsilon}{\partial r}\right) + \overline{u'v'}\frac{2U}{r} \tag{11}$$

This turbulence model has five empirical constants. According to the recommendations of Launder and Spalding[14] the following values of the constants were used in this analysis.

c_μ	c_1	c_2	σ_k	σ_ϵ
0.09	1.44	1.92	1.0	1.3

For boundary layer flows, Chambers and Wilcox[27] suggest using 9/2, rather than the factor of 2, in the curvature term. The effect of changing this value was not found to be significant.

DIFFERENCE EQUATIONS AND SOLUTION PROCEDURES

General Iteration Procedure

The equations involved are a coupled set of nonlinear, partial differential equations. These equations are transformed into a corresponding set of finite difference equations that necessitate an iterative type of solution to obtain the velocity and pressure field. The iterative approach is needed because the coefficients in the basic differential equations also involve the velocities and pressures being sought. Figure 2 briefly depicts the overall iterative approach and this is followed by a more detailed discussion of the method of solution.

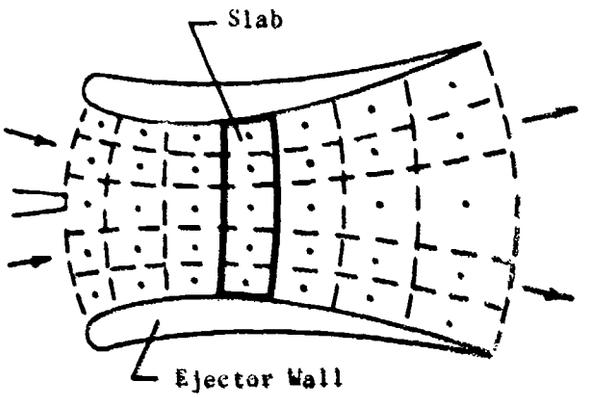

Step 1. Initialization
Estimate entire pressure and velocity field at problem start.

Step 2. Marching Solution for Velocities
Solve U-momentum equations for downstream U velocities.
Correct U's to satisfy overall mass continuity.
Solve continuity equation for V velocities.
Solve turbulence equations for k and ϵ yielding μ_t.
Repeat for next downstream slab.

Step 3. Solution for Entire Pressure Field
Solve Poisson's equation for pressures at each node.

Step 4. Convergence Check of Solution
Return to Step 2 if pressures and velocities are not converged.

Figure 2. General Solution Procedure

The major improvement in this approach is the manner in which the pressures are calculated. In the earlier method of Bevilaqua and DeJoode,[7] a single pass or march through the ejector was made. Pressures were stored in a single array in the program and downstream pressure effects could not be transmitted upstream. In the work of Pratap and Spalding[9,10] many passes were made through the duct and on each pass the downstream pressure perturbation was transmitted upstream over an incremental step distance. Convergence to the final pressure field was relatively slow. This is not the case for the program used herein. Pressures are stored in a two-dimensional array. The equations used to calculate all of the nodal pressures are solved in a simultaneous manner ("sweeping"). Any downstream effect is transmitted all the way upstream on each pass through the duct. Convergence is much faster.

Grid and Difference Equations

The notation for the velocities, U and V, and their control volumes follow the same general procedure used by Pratap, et al[10]. The control volumes are staggered as shown in Figure 3 and the subscripts P, N, S and E refer to the particular variables directed toward these nodal points. The notation N, S, E and W designate the points to the North, South, East and West.

Using this notation the continuity and momentum equations can be expressed in a simplified form.

Mass Conservation:

$$(\rho U_P) \cdot \text{Area} - (\rho U_E) \cdot \text{Area} + (\rho V_P) \cdot \text{Area} - (\rho V_N) \cdot \text{Area} = 0$$

U Momentum:

$$A_P^U U_P = A_N^U U_N + A_W^U U_W + A_S^U U_S + (P_W - P_P) \cdot \text{Area} + \text{Source} \cdot \text{Volume} \quad (12)$$

V Momentum:

$$A_P^V V_P = A_N^V V_N + A_W^V V_W + A_S^V V_S + (P_S - P_P) \cdot \text{Area} + \text{Source} \cdot \text{Volume}$$

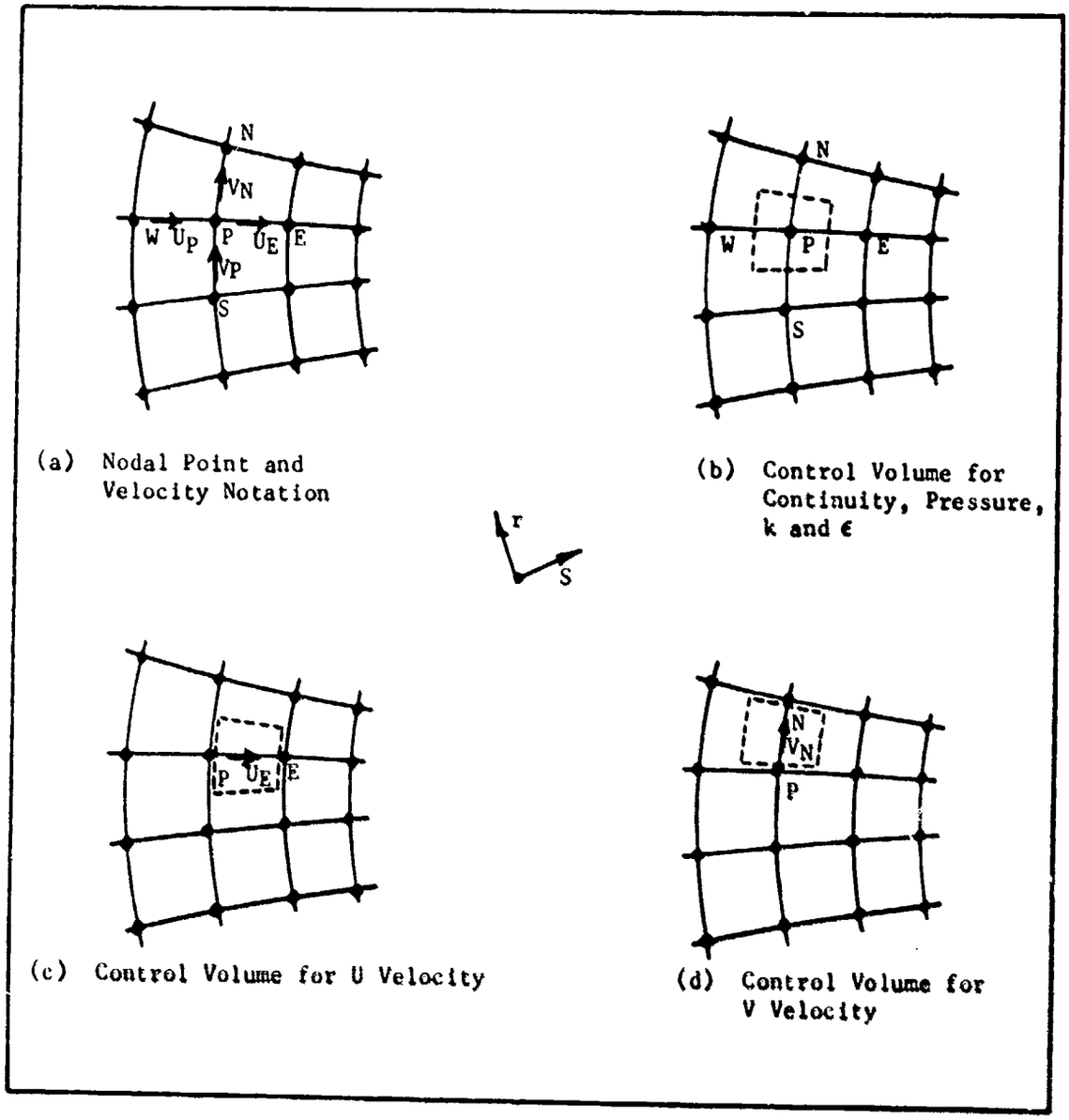

Figure 3. Grid, Velocity and Control Volume Notation

where the coefficients, A, represent the combined effects of convection and diffusion while the source terms include the effects of curvature, etc. The area terms correspond with the incremental volume surface over which the velocity or pressure is acting. To greatly simplify the computer program logic, Patankar[16] has suggested that both the momentum and turbulence equations be expressed in the simplified form:

$$\underbrace{\rho U \frac{\partial \phi}{\partial S} + \rho V \frac{\partial \phi}{\partial r}}_{\text{Convection}} = \underbrace{\frac{\partial}{\partial r}\left(\Gamma \frac{\partial \phi}{\partial r}\right)}_{\text{Diffusion}} + \text{Source} \qquad (13)$$

in which the symbol ϕ can represent U, V, k or ϵ as shown in Table I.

Table I. Generalized Equation Parameters

Equation	ϕ	Γ	Source
U Momentum	U	μ_t	$-\frac{\partial P}{\partial S} - \frac{U}{r^2}\frac{\partial}{\partial r}(\mu_t r) - \frac{\rho UV}{r}$
V Momentum	V	0	$-\frac{\partial P}{\partial r} + \frac{\rho U^2}{r}$
Turbulent Kinetic Energy	k	μ_t/σ_k	$G - \rho\epsilon - \frac{9}{2}\mu_t \frac{U}{r}\frac{\partial U}{\partial r}$
Rate of Dissipation of Turbulent Kinetic Energy	ϵ	μ_t/σ_ϵ	$\left(C_1 G - C_2 \rho\epsilon - \frac{9}{2}\mu_t \frac{U}{r}\frac{\partial U}{\partial r}\right)\frac{\epsilon}{k}$

Using the source term notation of Table I, Equation (13) can be expressed in a general finite difference form as:

$$A_P \phi_P = A_N \phi_N + A_W \phi_W + A_S \phi_S + \text{Source} \cdot \text{Volume} \qquad (14)$$

in which the subscripts refer to the nodal points in Figure 3. To insure mathematical stability, the "Source" terms in the above equation should

contain only the positive values of those shown in Table I while the negative source terms should be substituted into the A_P relation:

$$A_P = A_N + A_W + A_S - \text{Source} \cdot \text{Volume} \tag{15}$$

The terms A in this equation represent a combination of diffusion, d, and convection, C. For example, the diffusion from point P to N (Figure 3) for use in the U momentum equation can be described as:

$$d_N = \frac{\text{Area}}{\frac{\delta N}{\mu_{t_N}} + \frac{\delta P}{\mu_{t_P}}} \tag{16}$$

in which the interfacial area term, Area, is located at a distance, δ_N, from the N grid point and distances δ_P, from the P grid point. Although the turbulent viscosity is shown in Equation (16), laminar values can be used.

There is also a convective flow, C_N from nodal point, P, to N.

$$C_N = \rho \cdot \text{Area} \cdot V \tag{17}$$

To insure a more rapid and stable convergence in the iterative solution, Patankar[17,18] has developed the following relations for use in Equations (14) and (15).

$$A_N = a_N + \left[-C_N, 0\right]$$

where

$$a_N = d_N \left(1 - .1 \left|C_N\right|/d_N\right)^5 \quad \text{for } \left|C_N\right| < 10\, d_N \tag{18}$$

$$a_N = C_N \quad \text{for } \left|C_N\right| \geq 10\, d_N$$

in which the brackets, $[\ ]$, signify the largest of the two enclosed factors. In like manner, the combined diffusion and convection term, A_S, between nodes S and P are:

$$A_S = a_S + \left[C_S,\ 0\right] \tag{19}$$

The coefficient A_W in Equations (14) and (15) represents the convection on the west side of the control volume:

$$A_W = \rho \cdot \text{Area} \cdot U_W \tag{20}$$

In practice, the values of the diffusion and convection terms are averaged over two adjacent control volumes. It is recommended that reference to Patankar[17,18] be made for a more detailed description.

The marching technique (Figure 2) starts with the first slab and proceeds downstream, slab by slab. For example, the A_P, A_N, A_S, A_W along with the source terms are calculated for each cell in the particular slab considered. The unknown U velocities (Equation (14) with ϕ set to U) in the slab are calculated using a tridiagonal matrix algorithm with the velocity at the wall set to zero for the wall friction case. These U velocities generally do not satisfy the requirements of continuity over the entire slab (unless the convergence of all the momentum and turbulence equations is obtained) and an adaptation of the method of Sparrow, et al[19] is used to "adjust" the U velocities to satisfy slab overall continuity.

The V velocities are then calculated for each cell in the slab, Figure 4, starting with the lowest cell, using the basic continuity equation (constant density).

$$V_{out} = \frac{U_{in} \cdot \text{Area}_{in} - U_{out} \cdot \text{Area}_{out} + V_{in}\,\text{Area}_{in}}{\text{Area}_{out}} \tag{21}$$

in which the indicated areas correspond with the velocities. It will be shown later that the converged values of V depend on both continuity and the radial momentum equation (Equation 1).

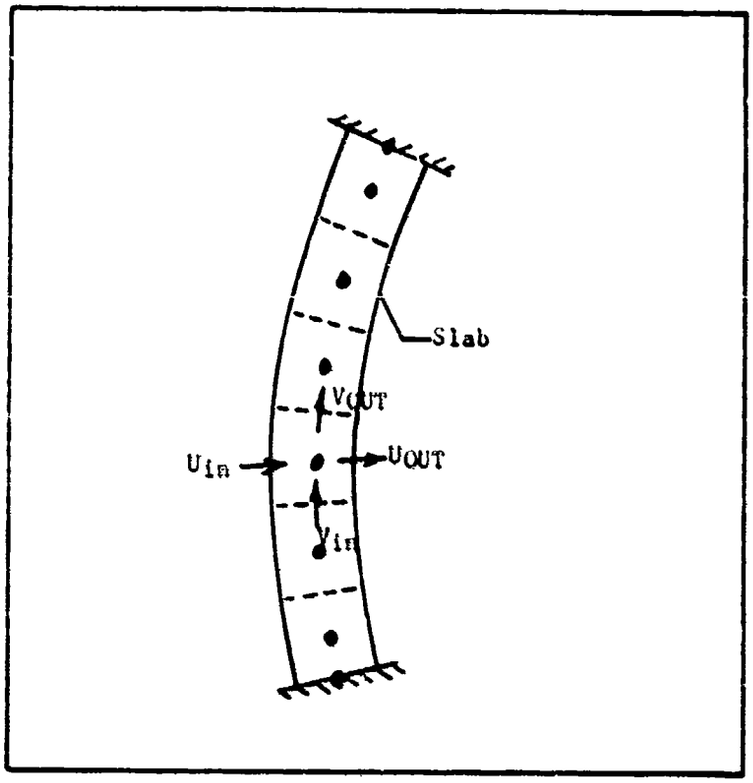

Figure 4. Slab Continuity

For the particular slab, the values of U and V are continually being updated. Using the "most recent" values, the turbulent kinetic energy, k, and dissipation, ϵ, equations are solved (Table I and Equations 8 through 11) in a similar manner as the U momentum equations. The newly calculated values of k and ϵ for each cell are then substituted into Equation (5) to determine the turbulent viscosity, μ_t, for the particular cell.

This entire procedure is repeated for each succeeding slab until the augmenter exit is reached. At this point in the iteration process, an estimate of the entire flow field of U and V velocities is known, although these values may not be the final, converged values.

Pressure Scheme

Before describing the detailed equations, it should be pointed out that there are two distinct improvements in the determination of the overall pressure field when compared with that done earlier (eg, Bevilaqua and DeJoode[7]). The first is that the pressure field in the program described in this paper involves an elliptic solution in that downstream pressures are transmitted to upstream regions. The second major improvement is the detachment of the pressure equation from the momentum equation in the solution. In the earlier approach a pressure correction was developed and was used to perform two tasks--correct the pressure and correct the velocity. This resulted in improved velocity distributions but relatively bad pressure fields in that convergence was slow. In the new improved approach, two separate equations are used, one to obtain the pressure (solution to Poisson type equation) and the other to correct the velocity. Test cases have shown that despite the extra numerical computations needed in the new procedure, there is a 30 to 50 percent saving in computer time.

The following paragraphs describe the procedure used for the calculation of the pressure field. These pressures are needed for substitution back into the momentum and turbulence equations to obtain an updated velocity field (Figure 1).

The U momentum equation has the form

$$A_P U_P = A_N U_N + A_W U_W + A_S U_S + \text{Source} \cdot \text{Vol} + \text{Area} \cdot (P_W - P_P) \qquad (22)$$

in which the area is the interfacial area perpendicular to the line extending from node point P_W to P_P (Figure 3). A_P is defined by Equation (15) and includes the convection/diffusion terms A_N, A_W, and A_S. Re-arranging Equation (22) leads to:

$$U_P = \left[\frac{A_N U_N + A_W U_W + A_S U_S + \text{Source} \cdot \text{Vol}}{A_P}\right] + \frac{\text{Area}}{A_P} (P_W - P_P) \qquad (23)$$

and replacing the bracketed term by $\hat{U}_P$ results in:

$$U_P = \hat{U}_P + \frac{\text{Area}}{A_P}(P_W - P_P) \tag{24}$$

In like manner (with different values of area)

$$U_E = \hat{U}_E + \frac{\text{Area}}{A_E}(P_P - P_E) \tag{25}$$

The V momentum equation:

$$V_P = \left[\frac{A_N V_N + A_W V_W + A_S V_S + \text{Source} \cdot \text{Vol}}{A_P}\right] + \frac{\text{Area}}{A_P}(P_S - P_P) \tag{26}$$

can also be simplified to:

$$V_P = \hat{V}_P + \frac{\text{Area}}{A_P}(P_S - P_P) \tag{27}$$

and

$$V_N = \hat{V}_N + \frac{\text{Area}}{A_N}(P_P - P_N) \tag{28}$$

The V_P and V_N relations represent the radial momentum equations. With the substitution of Equation (23) into the continuity equation for the pressure control volume (Figure 3):

$$(\rho U \text{ Area})_W - (\rho U \text{ Area})_E + (\rho V \text{ Area})_S - (\rho V \text{ Area})_N = 0 \tag{29}$$

there is obtained

$$A_P P_P = A_N P_N + A_W P_W + A_S P_S + A_E P_E + BB \tag{30}$$

in which

$$A_P = A_N + A_W + A_S + A_E \tag{31}$$

and

$$BB = (\rho \text{Area } \hat{U}_P) - (\rho \text{Area } \hat{U}_E) + (\rho \text{Area } \hat{V}_P) - (\rho \text{Area } \hat{V}_N) \tag{32}$$

With convergence the value of BB for each cell over the entire field approaches zero.

There are five unknowns in Equation (32); namely, the pressures at the center of the cell and the pressures of the four adjacent cells. When the number of cells in the flow field is large, it is expedient to solve for the pressures using a block relaxation technique followed by the use of the tridiagonal matrix algorithm sweeping from left to right, then right to left followed by sweeps in the vertical directions. For this study Patankar[17] developed a "block relaxation" technique that was shown to greatly accelerate convergence. In brief, a constant pressure correction is added to each slab prior to the sweeping action type computations.

The newly calculated pressures are then substituted back into the momentum and turbulence equations (Step 2 in Figure 2) and the entire procedure is repeated. Convergence is obtained when further calculations show that the values of velocity, k, ϵ, and pressure do not change within chosen tolerances.

Grid Generation

In order to calculate the velocity field in a non-uniform area duct, as in an augmenter, it is necessary to first generate a nearly orthogonal grid system, forming a set of "curvilinear squares" to which the finite difference equations can be applied. For accuracy, a large number of such squares or cells is desired. In the absence of a comprehensive computer program to perform this operation, the flow field in an augmenter was first subdivided into a coarse grid of squares by a trial-and-error, hand drawing technique (eg, Schneider[20]). Richardson[21] indicated agreement between graphical and exact analytical solutions of the order of 1.0 percent for simple, classical problems. The coarse grid for the augmenter analysis is presented in Figure 5. About midway through the augmenter, the "squares" were extended into rectangles for

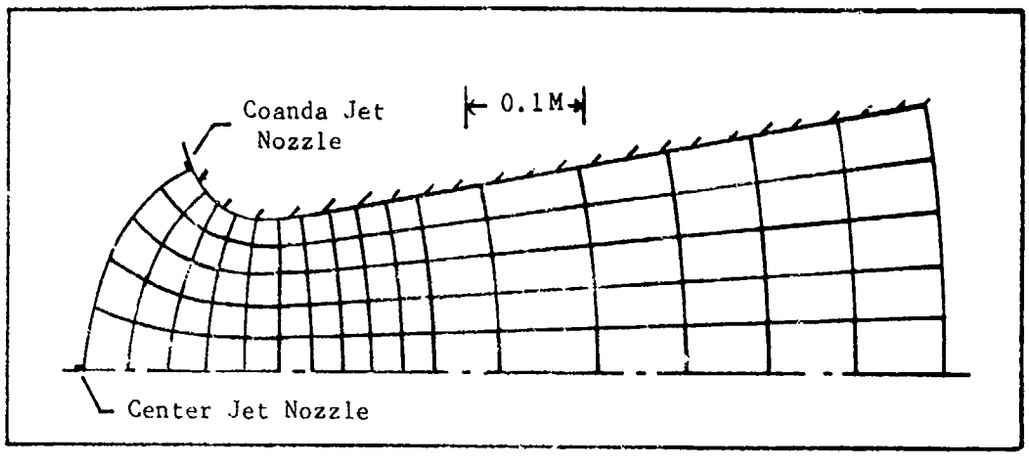

Figure 5. Orthogonal Squares Used in Ejector Flow Field Analysis

convenience in the computations. A computer program was written to further subdivided the coarse grid into a finer grid, consisting of a total of 3375 cells, 45 in the cross stream direction and 75 cells in the flow direction. The necessary geometric information for each of these cells was recorded on computer output tape for read-in to the viscous program. Results of the augmenter flow field calculations as well as some simpler test cases are presented in the following section.

RESULTS AND DISCUSSION

The comparison of experimental data with analytically predicted values from a computer program can be used to assess the accuracy of the mathematical modeling of the complex flow phenomenon. In this section comparisons are made for flow in straight ducts, as well as in curved ducts in order to demonstrate the cross stream (elliptic) pressure effect. Flow in an augmenter is also studied.

Flow in a Straight Duct

A comparison of predicted and measured velocities for fully developed turbulent flow in a 2-dimensional, parallel plate channel is shown in Figure 6. Good agreement with a mean line through the data of Laufer[22] is obtained.

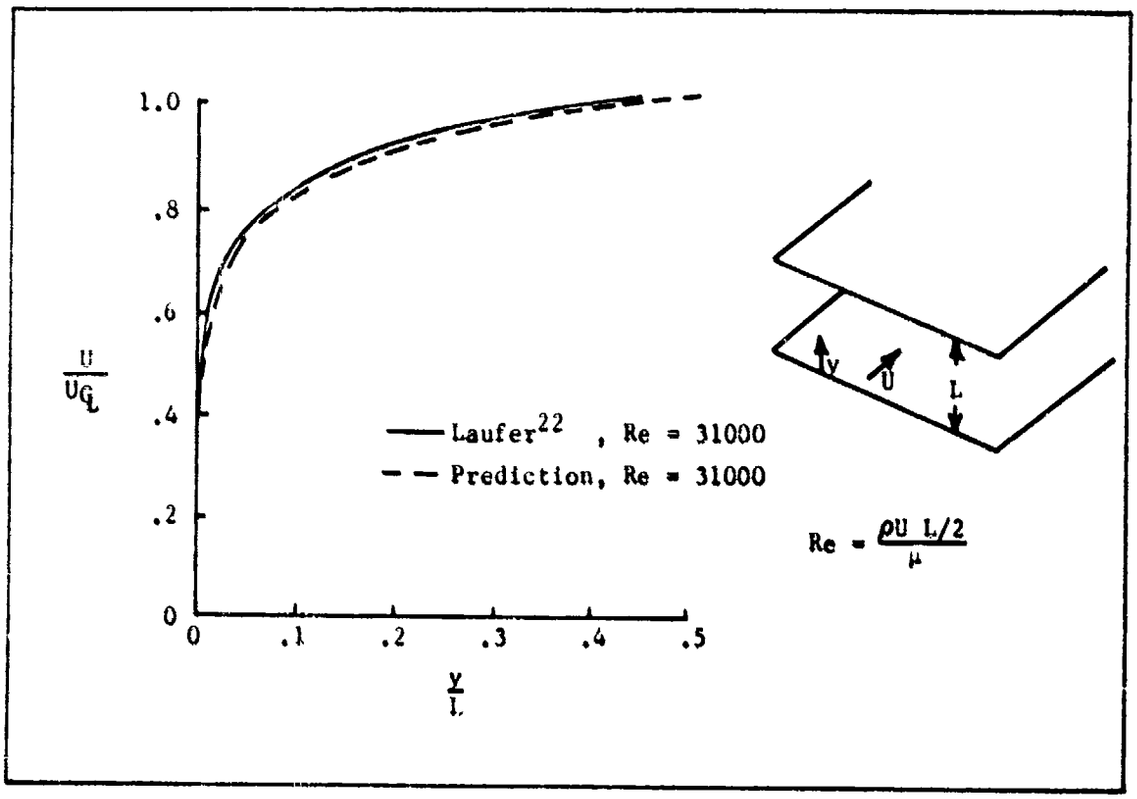

Figure 6. Comparison of Predicted and Measured Velocity Profiles for Fully Developed Turbulent Flow in a Channel

A similar comparison is shown in Figure 7 for the case of a plane turbulent jet in a co-flowing stream, the data being that of Weinstein,[23] et al. The initial jet velocity is twice that of the secondary flow, a value which is not too far different from that for augmenters.

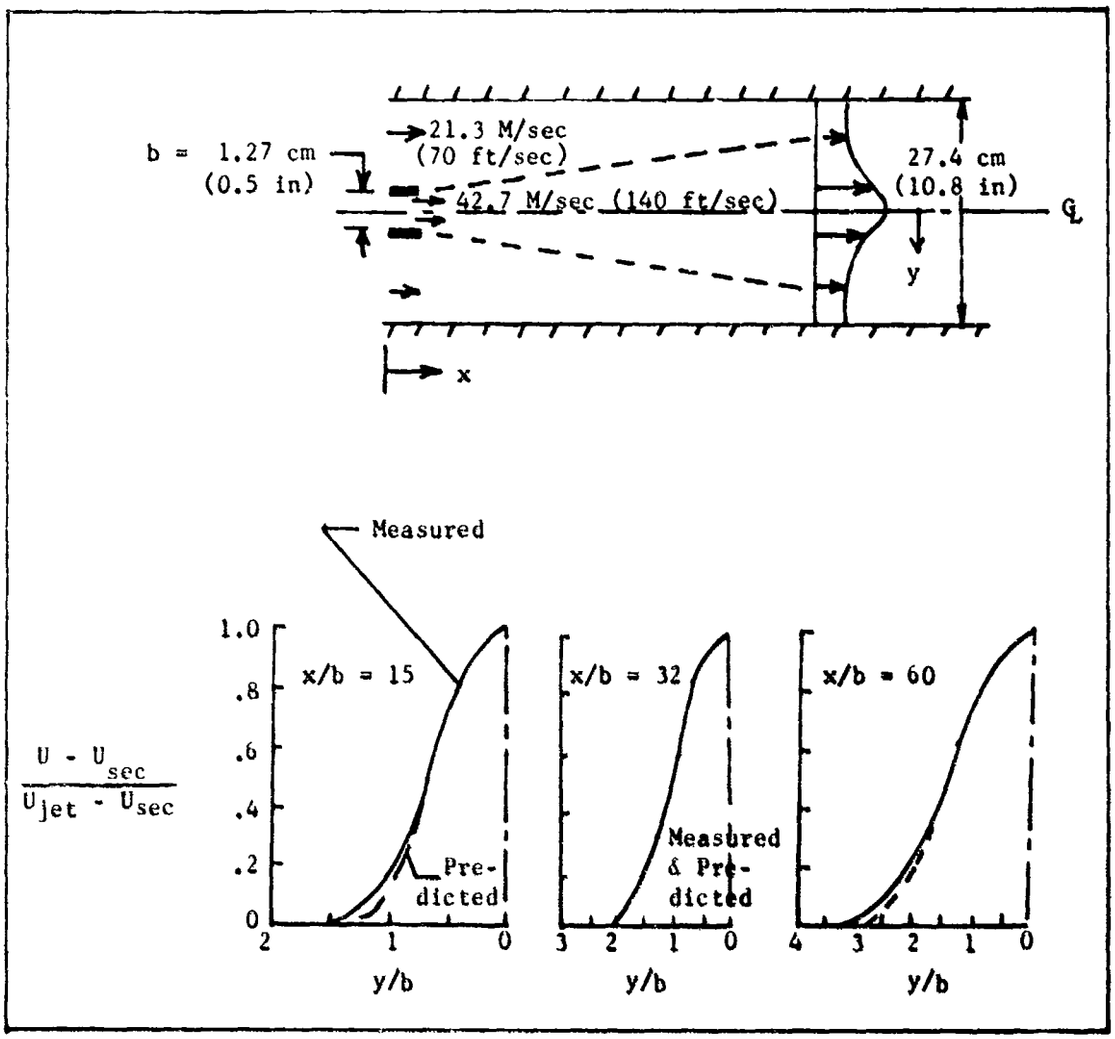

Figure 7. Comparison of Predicted and Measured Velocity Profiles for a Plane Turbulent Jet in a Co-flowing Stream

At distances to 60 jet widths, (the maximum investigated in the tests), the agreement is good. The slight differences at the outer edge of the jet might be attributed to the use of a "thick walled" nozzle in the experiment.

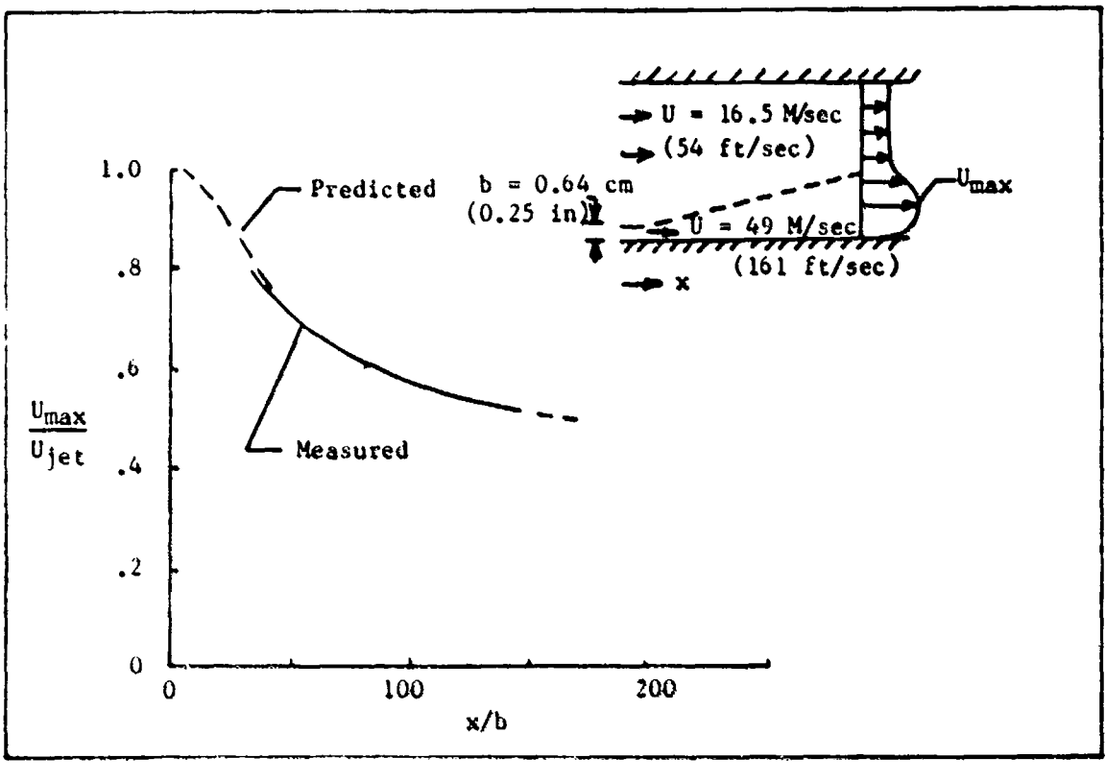

Figure 8. Comparison of Predicted and Measured Peak Velocities in a Turbulent Wall Jet in a Co-flowing Stream

The predicted decay of the maximum velocity of a wall jet in a co-flowing stream is compared in Figure 8 with the measured results of Gartshore and Newman[24]. Good agreement is also shown.

Flow in a Curved Duct

Although the program was primarily written to study turbulent mixing in ducts (augmenters) the program also has the capability for calculating laminar flow in ducts with and without curvature. The effect of curvature on fully developed, laminar flow is shown in Figure 9 for a duct with a high degree of curvature.

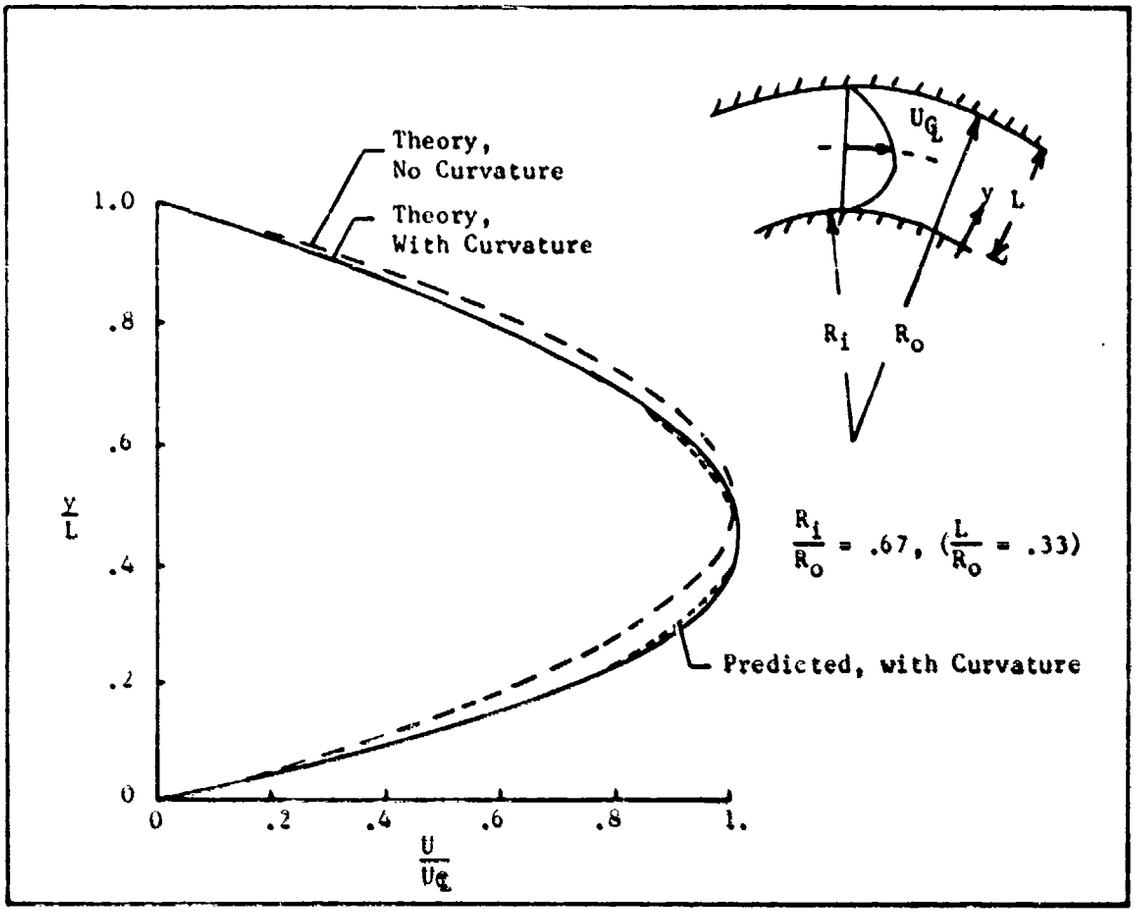

Figure 9. Comparison of Predicted Velocity Profiles with Mathematically Exact Theoretical Solutions for Fully Developed, Laminar Flow in 2-Dimensional Ducts with and without Curvature

Computer predicted values are in good agreement with the exact theoretical solution, developed by So[25]. As a matter of interest, the theoretical exact solution is also shown for the case where there is no curvature. For laminar flow it can be seen that the effect of curvature is small, which is not the case for turbulent flow.

The turbulent flow data of Eskinazi and Yeh[26] are used here for comparison with predicted values. The test configuration, Figure 10, consists of 4.88 meters (16 ft) straight duct preceeding the curved duct which

has a radius ratio of 0.9. This curvature is comparable to that for the flow of a Coanda jet over a curved surface in an augmenter. At the juncture

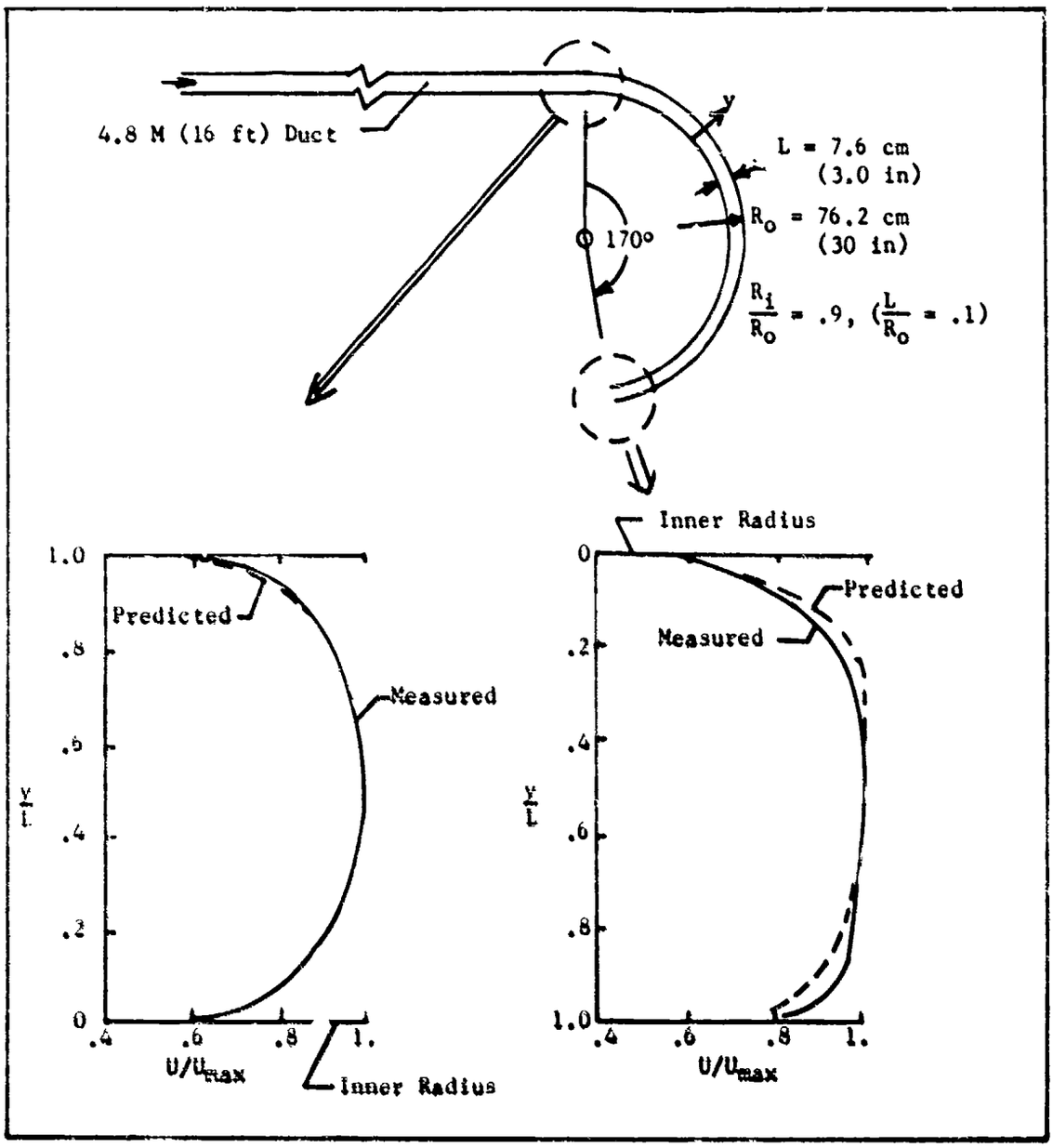

Figure 10. Comparison of Predicted and Measured Velocity Profiles for Turbulent Flow in a Rectangular, Curved Duct

of the straight and curved sections, predicted velocities agree well with a mean curve through the data. At the 170° station and inner surface ($y/L < .3$) predicted velocities are larger than measured values while at the outer surface ($y/L > .7$) the predicted values are smaller. The maximum difference in the calculated and measured velocities is of the order of 10 percent. Calculated pressures across the duct are in excellent agreement with measured values (Figure 11). The effect of curvature on the velocity profile is seen to be much larger for turbulent flow than laminar flow, when the results of Figures 9 and 10 are compared.

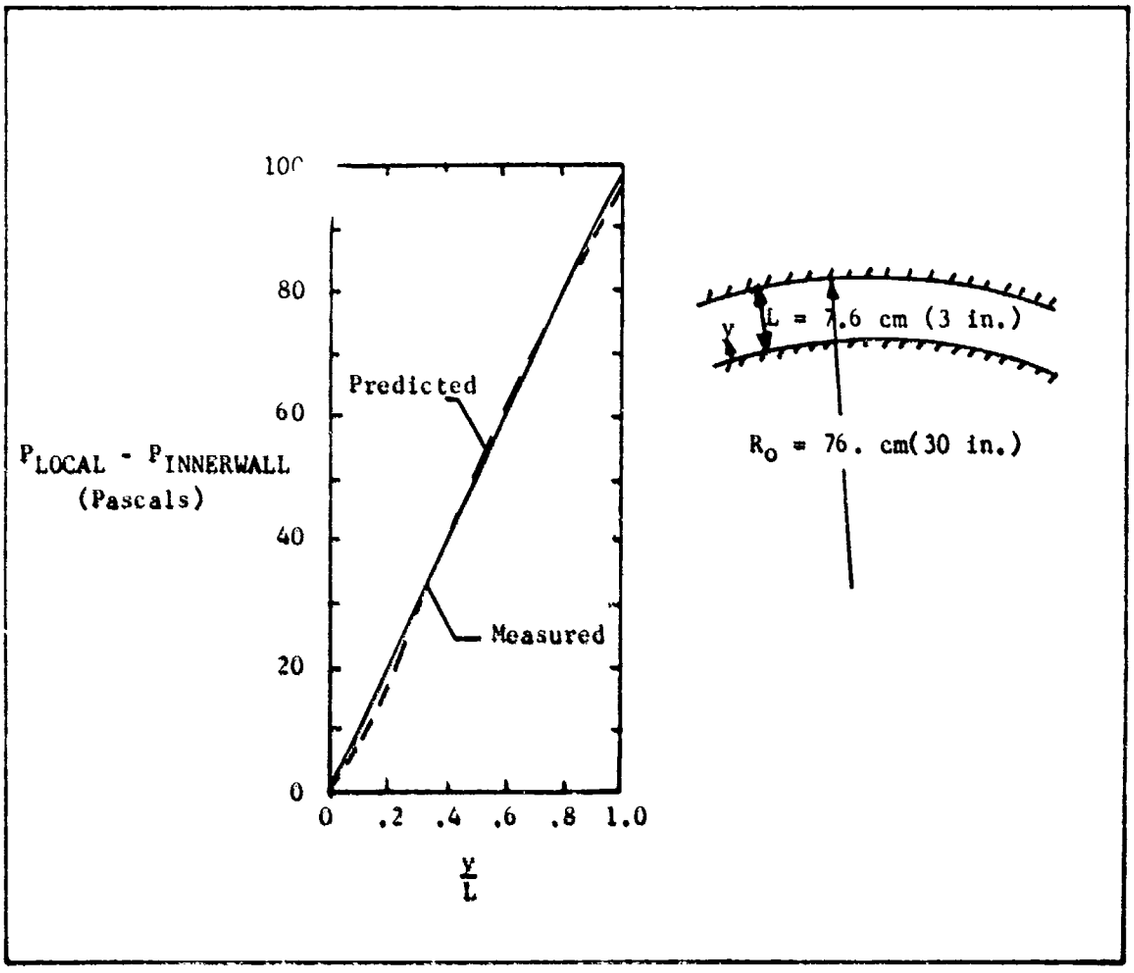

Figure 11. Comparison of Predicted and Measured Pressures for Turbulent Flow in Rectangular, Curved Duct.

Flow in an Ejector

The ejector model (Figures 5 and 12) has a throat width of 0.122 meters (0.4 ft) and a distance or length from the throat to the exit plane of 0.268 meters (0.88 ft). A characteristic geometric parameters is the ratio of this length to the ejector throat width. For this configuration the ratio of length-to-width is 2.2. The diffuser half angle is 10°. The center jet consists of a plane 2-dimensional slot jet with a total width

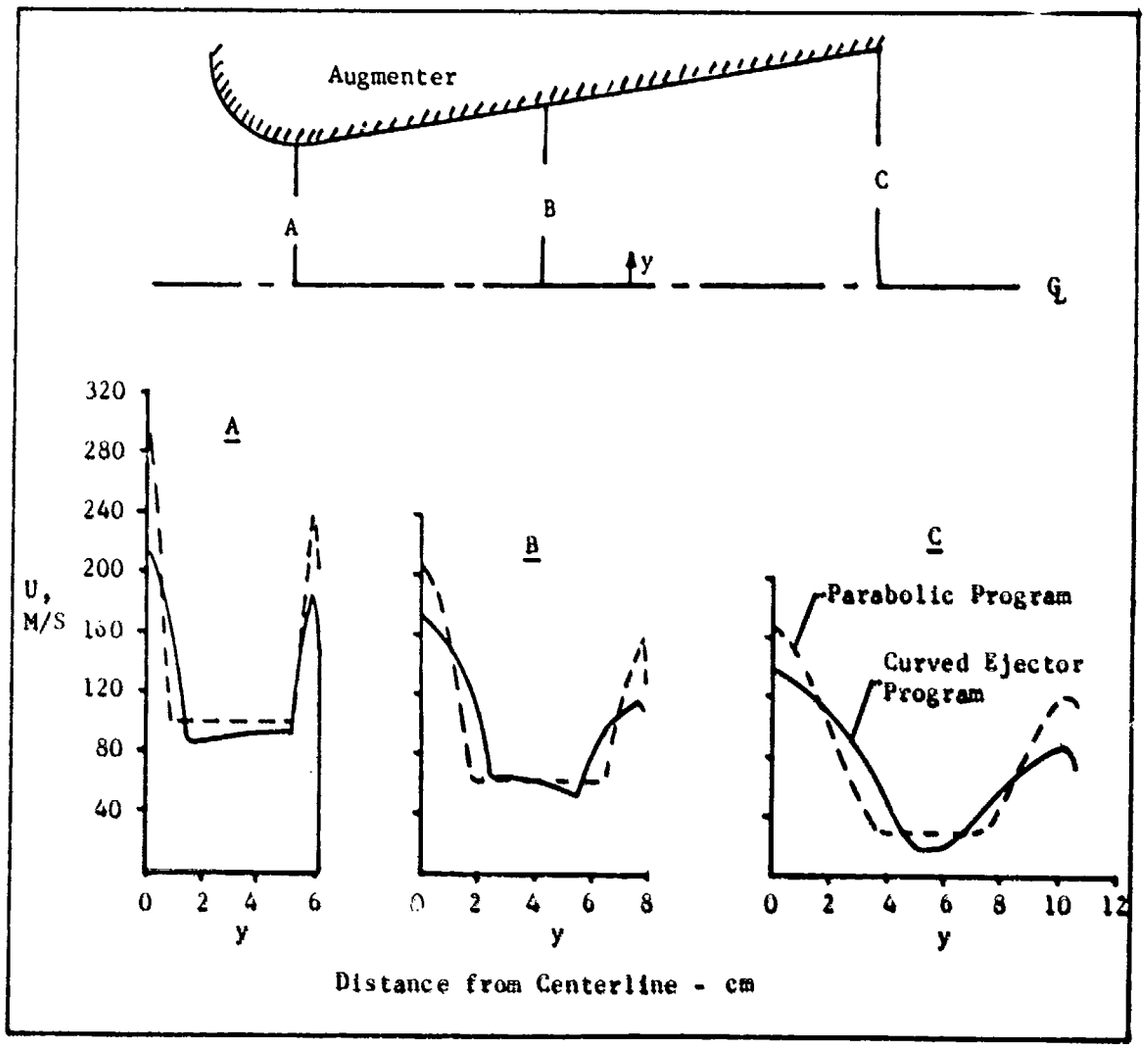

Figure 12. Comparison of the Cross Stream U Velocity Profiles Obtained from the Parabolic Program and the Curved Ejector Program

of 0.762 cm (0.3 in) while the Coanda gap is .191 cm (0.075 in). Nozzle exit velocities are 315.2 meters/sec (1034 ft/sec). The ratio of the radius of the Coanda surface to the Coanda gap is approximately 17.6 at the jet nozzle. Calculated velocities and cross stream pressure distributions, obtained from the curved ejector program, are shown for 3 stations. At the throat, Station A, the secondary velocity increases from 85.3 meters/sec (280 ft/sec) near the center jet at y = 1.37 cm (0.045 ft) to 94.5 meters/sec (310 ft/sec) near the Coanda jet at y = 5.18 cm (0.17 ft), the increase due to curvature. Over the same region the pressure in the secondary flow decreases from -4310. to -7180. pascals (-90 to

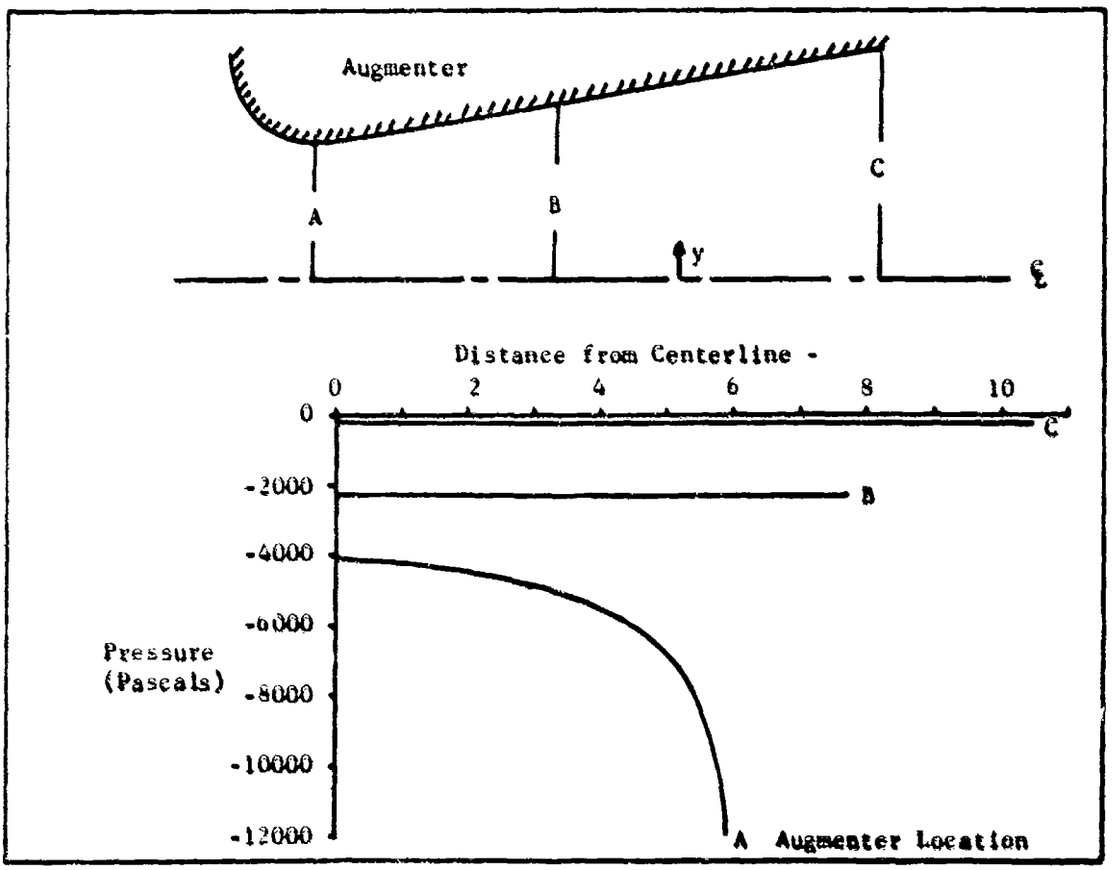

Figure 13. Variation of the Cross Stream Pressures Obtained from the Curved Ejector Program

-150 psfg) as shown in Figure 13 causing a V component or flow toward the Coanda surface and hence an increase in the U velocities.

At station B, the secondary velocities decrease with distance from the centerline, in contrast to that at station A. Curvature effects at station B are small (large radius of curvature) as indicated by the negligible cross stream pressure gradient in Figure 13 at this station. At the exit, the two jets are nearly merged and cross stream pressure gradients are likewise negligible.

For comparison purposes, the calculated velocities obtained with the parabolic flow program (Bevilaqua[7]) are also presented in Figure 12 in which the secondary mass flow rate is about 4 percent larger. This small difference in flow rates should have little effect on the overall trends. In the parabolic program, curvature in the flow field for ejector configurations cannot be accounted for nor can the downstream pressure effects have any influence on the upstream pressures and velocities (parabolic type solution). As a result, calculated secondary velocities are constant at any axial station, as shown. However, in the curved ejector programs the individual nodal pressures and corresponding velocities are interrelated over the entire flow field. In the comparison of center jet velocity profiles, it should be noted that the maximum or centerline velocities are larger for the parabolic program and this can be attributed to the relative axial location of the jet nozzle. In the parabolic program, the location of the center jet must be in the same plane as the Coanda nozzles. In the curved ejector program, the center jet is located upstream of the Coanda nozzle plane as indicated in Figure 5. With the center jet nozzle farther upstream, the downstream jet profile will be wider and have a lower peak velocity than that shown.

In the comparisons shown in Figure 12, the Coanda jet nozzles are in the same axial location in the ejector. Results for the curved ejector

program show a faster decay of the maximum wall jet velocity with a corresponding thickening of the wall jet. This is due to the addition of curvature effects because at station A there is a pressure decrease of approximately 4790 Pascals (100 psf) through the wall jet (from y = 5.2 to 5.94 cm). The effect of curvature on Coanda entrainment should be studied in more detail, in particular for Coanda surfaces having a small radius of curvatures. Although a symmetric ejector was analyzed in this paper, to permit comparison with the results of parabolic ejector programs, asymmetric configurations may also be analyzed with the scheme described here.

CONCLUSIONS

A viscous turbulent fluid flow program has been developed to extend the knowledge of the complex flow phenomena occurring in ejectors during the conversion or transition portion of the flight. For these conditions curvature of the flow through the ejector can cause a large pressure gradient across the duct, normal to the main flow direction. Because of this and its unknown effect on thrust, the curvature relations have been included in both the mean flow and turbulence equations to assess the effect of curvature on the flow field.

To establish a confidence level in the program, comparison cases were studied in which the program was used to calculate the velocities and pressures in straight as well as curved channels, and for wall jets and center jets located in a co-flowing stream. All of these flow cases can occur in an ejector. Such comparisons showed good agreement of predicted and measured data. For a static ejector the pressure gradients across the ejector channel were shown to be large. Curvature effects in the flow resulted in an increase in the spreading rate (increased entrainment) of the Coanda jet.

Based on the favorable results obtained with this program, it should prove very useful in the development of high performance augmenters, in particular when this viscous flow program is "inter-connected" with an inviscid program used for the calculation of the velocities outside of the ejector.

REFERENCES

1. Bevilaqua, P. M., "Lifting Surface Theory for Thrust Augmenting Ejectors," AIAA Journal, Vol. 16, No. 4, April 1978, p. 475.

2. Spence, D. A., "The Lift Coefficient of a Thin, Jet-Flapped Wing," Royal Society of London, Proceedings, Vol. 238, Jan. 1957, p. 46.

3. Chan, Y. Y., "Lift Induced by Suction Flaps on Augmenter Wings," Canadian Aeronautics and Space Institute Transactions, Vol. 3, No. 2, Sept. 1970, p. 107.

4. Woolard, H. W., "Thin-Airfoil Theory of an Ejector-Flapped Wing Section," AIAA Journal of Aircraft, Vol. 12, No. 1, Jan. 1975, p. 26.

5. Wilson, J. D., Loth, J. L., Chandra, S., "Thrust Augmented Wing Sections in Potential Flow," West Virginia University, Aerospace Engineering, TR-25, Aug. 1974.

6. Mendenhall, M. R. and McCillen, O. J., "Theoretical Analysis of an Augmenter Wing for a VTOL Fighter," Contract NAS2-9605, NASA Ames Research Center.

7. Bevilaqua, P. M. and DeJoode, A. D., "Viscid/Inviscid Interaction Analysis of Thrust Augmenting Ejectors," Office of Naval Research Report ONR CR212-249-1, Feb. 1978.

8. Gilbert, G. B. and Hill, P. G., "Analysis and Testing of Two-Dimensional Slot Nozzle Ejectors with Variable Area Mixing Sections," NASA CR-2251, May 1973.

9. Pratap, V. S. and Spalding, D. B., "Numerical Computation of the Flow in Curved Ducts," The Aeronautical Quarterly, Aug. 1975, p. 219.

10. Pratap V. S. and Spalding, D. B., "Fluid Flow and Heat Transfer in Three-Dimensional Duct Flows," Int. Journal of Heat Mass Transfer, Vol. 19, 1976, p. 1183.

11. Prandtl, L., "Effect of Stabilizing Forces on Turbulence," NACA Tech. Memorandum No. 625, 1931.

12. Townsend, A. A., "Entrainment and the Structure of Turbulent Flow," Journal of Fluid Mechanics, Vol. 41, 1970, pp. 13-46.

13. Bradshaw, P., "Review-Complex Turbulent Flows," ASME Trans., June 1975.

14. Launder, B. E. and Spalding, D. B., "Mathematical Models of Turbulence," Academic Press, 1972.

15. Hunt, I. A. and Joubert, P. N., "Effects of Small Streamline Curvature on Turbulent Duct Flow," Journal of Fluid Mechanics, Vol. 91, 1979, pp. 633-659.

16. Patankar, S. V., "Numerical Solution of Heat Transfer and Fluid Flow," Course Notes Presented at the Dec. 11, 1978 ASME Winter Meeting in San Francisco, CA.

17. Patankar, S. V., "Numerical Heat Transfer and Fluid Flow," Hemisphere Publishing Co., New York, New York, 1980.

18. Patankar, S. V., "A Calculation Procedure for Two-Dimensional Elliptic Situations," (to be published in Numerical Heat Transfer, Vol. 2.).

19. Sparrow, E. M., Baliga, B. R., and Patankar, S. V., "Heat Transfer and Fluid Flow Analysis of Interrupted Wall Channels with Application to Heat Exchangers," Journal of Heat Transfer, Feb. 1977, Vol. 99.

20. Schneider, P. J., "Conduction Heat Transfer," Addison-Wesley Publishing Co., Inc., 1955.

21. Richardson, L. F., "A Freehand Graphic Method of Determining Stream Lines and Equipotentials," Philosophical Magazine, Ser. 6, 15.

22. Laufer, J., "Some Recent Measurements in a Two-Dimensional Turbulent Channel," Journal of the Aeronautical Sciences, May 1950.

23. Weinstein, A., Osterle, J., and Forstall, W., "Momentum Diffusion from a Slot Jet into a Moving Secondary," Journal of Applied Mechanics, Sept. 1976.

24. Gartshore, I. and Newman, B., "The Turbulent Wall Jet in an Arbitrary Pressure Gradient," Aeronautical Quarterly, Feb. 1969.

25. So, R. M., "Entry Flow in Curved Channels," Journal of Fluids Engineering, June 1976.

26. Eskinazi, S. and Yeh, H., "An Investigation of Fully Developed Turbulent Flows in a Curved Channel," Journal of Aeronautical Science, Vol. 23, Jan. 1956.

27. Chambers, T and Wilcox, D., "Critical Examination of Two-Equation Turbulence Closure Models," AIAA Paper 76-352, July 1976.

DISTRIBUTION LIST

Office of Naval Research
800 N. Quincy St.
Arlington, VA 22217
- ONR 211 — 4
- ONR 430B — 1

Office of Naval Research Branch Office
1030 E. Green St.
Pasadena, CA 91106 — 1

Office of Naval Research Branch Office
Bldg. 114 Section D
666 Summer St.
Boston, MA 02210 — 1

Office of Naval Research Branch Office
536 South Clark St.
Chicago, IL 60605 — 1

Naval Research Laboratory
Washington, DC 20375
- Code 2627 — 1
- Code 2629 — 1

Defense Technical Information Center
Bldg. 5 Cameron Station
Alexandria, VA 22314 — 12

Naval Air Systems Command
Washington, DC 20361
- AIR 320D (Mr. D. Kirkpatrick) — 1
- AIR 5301-33B (Mr. Lynn Trobaugh) — 1
- AIR 03PA (H. Andrews) — 1
- AIR ADPO-16 (CDR J. Farley) — 1

Naval Air Development Center
Warminster, PA 18974
- Code 6053 (Mr. C. Mazza) — 2

David Taylor Naval Ship Research and Development Center
Bethesda, MD 20084
- Code 16 (Dr. H. Chaplin) — 1
- Code 1660 (Mr. J. Nichols) — 1
- Code 522.3 Aero Library — 1

U. S. Naval Postgraduate School
Monterey, CA 93940
- Dept. of Aeronautics (Code 57) — 1
- Library — 1

Superintendent
U. S. Naval Academy
Annapolis, MD 21402 — 1

NASA Ames Research Center
Moffett Field, CA 94035
- FAE Branch (Dr. T. Gregory) — 1
- Mr. D. Keonig — 1

NASA Langley Research Center
Hampton, VA 23665
- Mr. R. Margason — 1

Wright Patterson Air Force Base
Dayton, OH 45433
- Aero & Airframe Branch (Dr. T. Weeks) — 1

Air Force Office of Scientific Research
Bolling AFB, DC 20332
- Code NA (Dr. J. Wilson) — 1

Lockheed Missiles & Space Co., Inc.
Huntsville Research & Engineering Center
P. O. Box 1103
Huntsville, AL 35807
- Mr. A. Zalay — 1

Nielsen Engineering & Research, Inc.
510 Clyde Avenue
Mountain View, CA 94043 — 1

McDonnell Douglas Aircraft Company
P. O. Box 516
St. Louis, MO 63166
- Aerodynamics (Dr. D. Kotansky) — 1
- Propulsion (Mr. J. Kamman) — 1

Vought Corporation
Advanced Technology Center, Inc.
P. O. Box 6144
Dallas, TX 75222
- Dr. C. S. Wells, Jr. — 1

Grumman Aerospace Corporation
Bethpage, NY 11714
Research Dept. (Dr. R. Melnik) 1
Advanced Dev. Dept. (Mr. F. Berger) 1

University of Southern California
Dept. of Aerospace Engineering
University Park
Los Angeles, CA 90007
Prof. John Laufer 1

Virginia Polytechnic Institute
Dept. of Engr. Sciences & Mechanics
Blacksburg, VA 24061 1

University of Maryland
Dept. of Aerospace Engr.
College Park, MD 20742
Dr. J. D. Anderson, Jr. 1

United Aircraft Corporation
Research Laboratories
Silver Lane
East Hartford, CT 06108
Dr. M. Werle 1

Polytechnic Institute of New York
Long Island Center
Dept. of Aero Engr. and Applied Mechanics
Route 110
Farmingdale, NY 11735 1

Scientific Research Associates, Inc.
P. O. Box 498
Glastonbury, CT 06033
Dr. H. McDonald 1

Douglas Aircraft Company
3855 Lakewood Blvd.
Long Beach, CA 90808
Dr. T. Cebeci 1

General Dynamics/Fort Worth Div.
Aerospace Tech. Dept.
Fort Worth, TX 76101
Dr. W. Foley 1